Hardware-Efficient Quantum Random Access Memory with Hybrid Quantum Acoustic Systems

Connor T. Hann, Chang-Ling Zou, Yaxing Zhang, Yiwen Chu, Robert J. Schoelkopf, S. M. Girvin, and Liang Jiang

Phys. Rev. Lett. **123**, 250501 — Published 17 December 2019

DOI: 10.1103/PhysRevLett.123.250501

Hardware-efficient quantum random access memory with hybrid quantum acoustic systems

Connor T. Hann,[1] Chang-Ling Zou,[2] Yaxing Zhang,[1] Yiwen Chu,[3] Robert J. Schoelkopf,[1] S. M. Girvin,[1] and Liang Jiang[1]

[1] *Departments of Applied Physics and Physics, Yale University, New Haven, Connecticut 06511, USA*
[2] *Key Laboratory of Quantum Information, CAS, University of Science and Technology of China, Hefei, China.*
[3] *Department of Physics, ETH Zürich, 8093 Zürich, Switzerland*

Hybrid quantum systems in which acoustic resonators couple to superconducting qubits are promising quantum information platforms. High quality factors and small mode volumes make acoustic modes ideal quantum memories, while the qubit-phonon coupling enables the initialization and manipulation of quantum states. We present a scheme for quantum computing with multimode quantum acoustic systems, and based on this scheme, propose a hardware-efficient implementation of a quantum random access memory (qRAM). Quantum information is stored in high-Q phonon modes, and couplings between modes are engineered by applying off-resonant drives to a transmon qubit. In comparison to existing proposals that involve directly exciting the qubit, this scheme can offer a substantial improvement in gate fidelity for long-lived acoustic modes. We show how these engineered phonon-phonon couplings can be used to access data in superposition according to the state of designated address modes—implementing a qRAM on a single chip.

Introduction.—The coupling of superconducting qubits to microwave resonators, termed circuit quantum electrodynamics (cQED) [1, 2], constitutes one of today's most promising quantum computing architectures. Microwave modes provide good quantum memories [3], while superconducting nonlinearities enable the initialization [4], manipulation [5, 6], readout [7], and protection [8, 9] of quantum states encoded in microwave photons. However, long microwave wavelengths could potentially limit the scalability of cQED systems. On-chip resonators face trade-offs between compactness and quality factor [10, 11], and microwave modes with millisecond coherence have thus far only been demonstrated in large 3D cavities [3, 12].

Recently, coherent couplings between superconducting qubits and acoustic resonators have been demonstrated in a remarkable series of experiments [13–25]. These so-called circuit quantum acoustodynamic (cQAD) systems (Fig. 1) possess many of the advantageous properties of cQED systems, e.g., superconducting qubits can be used to generate arbitrary superpositions of acoustic Fock states [17, 21] and perform phonon-number resolving measurements [24, 25]. Yet relative to electromagnetic modes, acoustic modes can provide dramatic benefits in terms of size and coherence times. The velocities of light and sound differ by five orders of magnitude, and short acoustic wavelengths enable the fabrication of ultra-compact phononic resonators [26]. Furthermore, acoustic modes can be exceptionally well-isolated from their environments—quality factors in excess of 10^{10} were recently demonstrated in GHz frequency phononic crystal resonators [27]. A variety of applications for such platforms have been proposed, including quantum transduction [28], entanglement generation [29, 30], and quantum signal processing [31, 32], but surprisingly the direct use of cQAD systems for quantum computing has received relatively little attention, with the notable exception of Ref. [33].

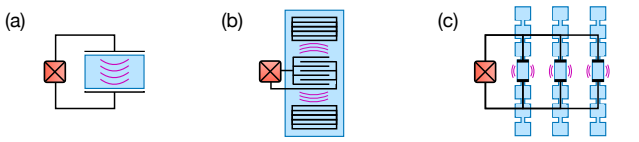

FIG. 1. Multimode cQAD. A transmon qubit (red) is piezoelectrically coupled to (a) a bulk acoustic wave resonator, (b) a surface acoustic wave resonator, or (c) an array of phononic crystal resonators.

In this work, we propose a hardware-efficient and scalable quantum computing architecture for multimode cQAD systems. Quantum information is stored in high-quality acoustic modes, and interactions between modes are engineered by applying off-resonant drives to an ancillary superconducting transmon qubit. During these operations, the transmon is only virtually excited, so the effects of transmon decoherence are mitigated. This is a crucial property, since the transmon's decoherence rate can exceed that of the phonons by orders of magnitude. In comparison to existing proposals that involve directly exciting the transmon [33, 34], this virtual approach can offer substantial improvement in gate fidelity for long-lived phonons. This scheme is also directly applicable to multimode cQED [34].

Furthermore, to demonstrate the benefits that the proposed cQAD architecture affords in hardware efficiency, we propose an implementation of a quantum random access memory (qRAM) [35, 36]. A classical RAM is a device that can query a database. Given an address j as input, the RAM outputs the element D_j stored at posi-

tion j in the database. Analogously, a qRAM is a device that, when provided with a superposition of addresses, returns a correlated superposition of data,

$$\sum_{j=1}^{N} \alpha_j \left|j\right\rangle_a \left|0\right\rangle_b \xrightarrow{\text{qRAM}} \sum_{j=1}^{N} \alpha_j \left|j\right\rangle_a \left|D_j\right\rangle_b , \tag{1}$$

where the subscripts a and b denote the address and output qubit registers, respectively. The ability to perform such queries efficiently, i.e. in $\log N$ time, is a prerequisite for a variety of quantum algorithms that provide speedups over their classical counterparts [37–39]. However, building a qRAM is highly non-trivial; even a small-scale qRAM of the sort described in Ref. [35] has yet to be experimentally demonstrated. One major challenge is that, to query a database of size N, a qRAM requires $O(N)$ quantum resources [36]. Hardware-efficiency is thus crucial for qRAM queries of large datasets, and in our implementation this efficiency is enabled by the on-chip integration of superconducting circuits with compact acoustic resonators. Out proposal both reduces physical resource requirements and provides a roadmap for a near-term demonstration of qRAM.

Note that "random access quantum memories" [34, 40, 41]—memories that can take a single *classical* address j as input and return a corresponding qubit $|\psi_j\rangle$—cannot generally perform operation (1) and should not be confused with qRAM, which can use superpositions of addresses to query multiple memory elements.

Quantum computing in cQAD.—In multimode cQAD, a transmon qubit is piezoelectrically coupled to a collection of acoustic modes. These modes can be supported in bulk acoustic wave (BAW) [16–18] or surface acoustic wave (SAW) [19–24] resonators, or in an array of phononic crystal (PC) resonators [25] (Fig. 1). Quality factors of $\approx 10^5$, 10^8, and 10^{10} have been measured at GHz frequencies in SAW [42, 43], BAW [44, 45], and PC resonators [27], respectively, and the transmon can be simultaneously coupled to many high-Q modes on a single chip [16]. These systems can be described by the Hamiltonian

$$\begin{aligned} H = \omega_q q^\dagger q - \frac{\alpha}{2} q^\dagger q^\dagger q q \\ + \sum_k \left(\omega_k m_k^\dagger m_k + g_k q^\dagger m_k + g_k^* q m_k^\dagger \right) + H_d \end{aligned} \tag{2}$$

Here, q and m_k denote the annihilation operators for the transmon and phonon modes, respectively. The transmon is modeled as an anharmonic oscillator with Kerr nonlinearity α and is coupled to the k^{th} phonon mode with strength g_k (typically a few MHz [19, 25, 46]). In combination with external drives on the transmon $H_d = \sum_j \Omega_j q^\dagger e^{-i\omega_j t} + \text{H.c.}$, this coupling provides the basic tool to initialize, manipulate, and measure phononic qubits [17, 21]. For example, itinerant photon-encoded qubits sent to the system can be routed into a particular phonon mode via pitch-and-catch schemes [47–51].

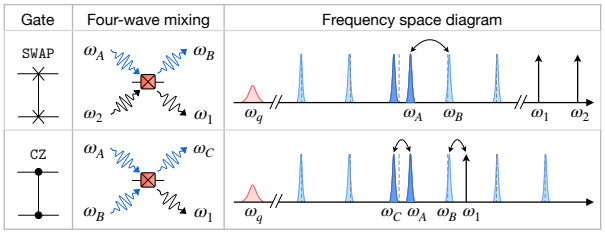

FIG. 2. Phonon-phonon gates. `SWAP`: Applying two drives with $\omega_2 - \omega_1 = \omega_B - \omega_A$ creates an effective coupling between modes A and B. `CZ`: Applying a single drive with $\omega_1 = \omega_A + \omega_B - \omega_C$ creates an effective three-mode coupling between modes A, B, and C. Frequency shifts of strongly hybridized modes (dark blue) can enable selective coupling when the modes are otherwise uniformly spaced (dashed lines denote uniform spacing) [56].

Interactions between phonon modes can be engineered by applying off-resonant drives to the transmon, and we use these interactions to implement a universal gate set for phononic qubits. The main idea is that the transmon's Kerr nonlinearity enables it to act as a four-wave mixer [52–55], so phonons can be converted from one frequency to another by driving the transmon. For example, phonons can be converted from frequency ω_A to ω_B by applying two drive tones whose frequencies $\omega_{1,2}$ satisfy the resonance condition $\omega_2 - \omega_1 = \omega_B - \omega_A$, see Fig. 2. This driving gives rise to an effective Hamiltonian $H = g_v^{(1)} m_A m_B^\dagger + \text{H.c.}$, where $g_v^{(1)} = -2\alpha \frac{g_A}{\delta_A} \frac{g_B^*}{\delta_B} \frac{\Omega_1^*}{\delta_1} \frac{\Omega_2}{\delta_2} (1 - \beta^{(1)})$. Here, $\delta_j \equiv \omega_j - \omega_q$, and $\beta^{(1)}$ is a drive-dependent correction (see supplementary material [56] for derivations). Evolution under this coupling for a time $\pi / 2 g_v^{(1)}$ implements a `SWAP` gate, which exchanges the states of modes m_A and m_B, while evolution for a time $\pi / 4 g_v^{(1)}$ implements a 50:50 beamsplitter operation [54].

Three-mode interactions can be similarly engineered (Fig. 2). Applying a single drive tone with frequency $\omega_1 = \omega_A + \omega_B - \omega_C$ gives rise to the effective Hamiltonian $H = g_v^{(2)} m_A m_B m_C^\dagger + \text{H.c.}$, where $g_v^{(2)} = -2\alpha \frac{g_A}{\delta_A} \frac{g_B}{\delta_B} \frac{g_C^*}{\delta_C} \frac{\Omega_1^*}{\delta_1} (1 - \beta^{(2)})$ [56]. This three-mode interaction can be used to implement a controlled phase (`CZ`) gate for qubits encoded in the $|0,1\rangle$ phonon Fock states [57]. To perform a `CZ` gate between qubits in modes A and B, mode C is used as an ancilla and initialized in $|0\rangle$. Evolving for a time $\pi / g_v^{(2)}$ then enacts the mapping $|110\rangle_{ABC} \to |001\rangle \to -|110\rangle$, while leaving all other initial states unaffected. The state $|11\rangle_{AB}$ acquires a relative geometric phase, thereby implementing the `CZ` gate.

A variety of other operations can be similarly implemented. Single- and two-mode squeezing can be implemented by driving the transmon at appropriate frequencies, and phase shifts can be imparted by tuning the drive phases during `SWAP` operations. Together, these two- and

three-mode interactions are universal [56, 58]. In the remainder of this work, however, we focus on the beamsplitter, `SWAP`, and `CZ` operations, as these are the only operations we require to implement a qRAM.

Note that in BAW and SAW resonators, phonon mode frequencies are approximately uniformly spaced, i.e. $\omega_{j+1}-\omega_j = \nu$, where ν is the free spectral range. This uniform spacing can lead to problematic degeneracies in the resonance conditions above. Nonuniform mode spacing is thus necessary to enable selective coupling, and in [56] we describe several ways to engineer nonuniformity in BAW and SAW systems. As shown in Fig. 2, one approach is to couple the phonons to an external mode, such as a microwave resonator, so that the resulting hybridization shifts mode frequencies [46]. In [56], we also introduce a metric, $\Delta\nu$, to quantify the nonuniformity. Roughly speaking, $\Delta\nu$ is the scale at which the mode spacing varies.

Gate fidelities.—During the gates described above, the transmon is never directly excited; instead, it is only *virtually* excited, so infidelity attributable to transmon decoherence is suppressed. These virtual gates can thus provide great advantage in cQAD systems, where transmon decoherence is likely to be the limiting factor. This is in contrast to existing proposals [33, 34], in which gates between resonator mode qubits are implemented by swapping information *directly* into the transmon using resonant interactions of the form $g_d(q^\dagger m + q m^\dagger)$, which can be engineered, e.g., by modulating the transmon's frequency. In the following, we compare the predicted fidelities of the *virtual* gates proposed here and the *direct* gates considered in Refs. [33, 34].

In a multimode architecture, there exists a fundamental tradeoff between decoherence and spectral crowding. Slower gates are more prone to decoherence, while faster gates have reduced frequency resolution and can disrupt other modes. The infidelities of the direct and virtual gates, respectively $1-\mathcal{F}_d$ and $1-\mathcal{F}_v$, can be approximated as a sum of contributions from these two effects [33, 56],

$$1-\mathcal{F}_d \approx (\kappa+\gamma)\frac{c_d\pi}{2g_d} + \left(\frac{g_d}{\nu}\right)^2, \tag{3}$$

$$1-\mathcal{F}_v \approx \bar{\kappa}_\gamma\frac{c_v\pi}{2g_v} + \left(\frac{g_v}{\Delta\nu}\right)^2, \tag{4}$$

where κ and γ are the bare phonon and transmon decoherence rates, and $c_{d,v}$ are constants accounting for the durations of each gate ($c_v = 1$ for `SWAP`, and $c_v = 2$ for `CZ`, as these gates have durations $\pi/2g_v$ and π/g_v respectively. As discussed in Ref. [34], $c_d = 5$ for `SWAP` and $c_d = 4$ for `CZ`.)

The first terms in Eq. (3) and Eq. (4) account for decoherence. During direct gates, information spends roughly equal time in the phonon and transmon modes, so the total decoherence rate is $\kappa+\gamma$. During virtual gates, the total decoherence rate, $\bar{\kappa}_\gamma$, is $\bar{\kappa}_\gamma = (\kappa_\gamma^A + \kappa_\gamma^B)$ for `SWAP`, and $\bar{\kappa}_\gamma = (\kappa_\gamma^A + \kappa_\gamma^B + \kappa_\gamma^C)/2$ for `CZ`. Here, $\kappa_\gamma^j = \kappa + \gamma(g_j/\delta_j)^2(1+\beta^{(\gamma)})$ denotes the dressed decay rate of mode j, which includes a contribution from the inverse Purcell effect [3, 55] and a drive-dependent correction $\beta^{(\gamma)}$ [56]. The second term in each expression accounts for spectral crowding. The probability of accidentally exciting another mode scales as $(g_d/\nu)^2$ in the direct case, and as $(g_v/\Delta\nu)^2$ in the virtual case. We note that the infidelities (3,4) are defined with respect to the ideal *two-qubit* unitaries; see [56] for derivations.

The competition between decoherence and spectral crowding results in an optimal coupling rate [33]. By adjusting the drive strengths, $g_{d,v}$ can be tuned to their respective optima. The optimal infidelities are

$$1-\mathcal{F}_d \approx \frac{3}{2}\left[\frac{c_d\pi(\kappa+\gamma)}{\sqrt{2}\nu}\right]^{2/3}, \tag{5}$$

$$1-\mathcal{F}_v \approx \frac{3}{2}\left[\frac{c_v\pi\bar{\kappa}_\gamma}{\sqrt{2}\Delta\nu}\right]^{2/3}. \tag{6}$$

While transmon and phonon decoherence contribute equally to $1-\mathcal{F}_d$, transmon decoherence only makes a small contribution to $1-\mathcal{F}_v$ via the inverse Purcell effect, wherein γ is suppressed by a factor of $(g/\delta)^2 \ll 1$. The virtual gates can thus be expected to attain higher fidelities when there is a large disparity between γ and κ, i.e. for sufficiently long-lived phonon modes. Indeed, $\mathcal{F}_v > \mathcal{F}_d$ whenever $\kappa_\gamma \lesssim (\kappa+\gamma)\Delta\nu/\nu$, provided the optimal coupling rates can be reached.

In Fig. 3, we plot the optimal infidelities of direct and virtual gates as a function of κ and γ for currently feasible experimental parameters. The comparison reveals that virtual gates can be performed with high fidelity (>99%) given long-lived phonons, and that virtual gates attain higher fidelities than direct gates in the same regime. Indeed, realistic improvements in phonon coherence are likely to bring near-term devices into this $\mathcal{F}_v \gg \mathcal{F}_d$ regime (Fig. 3c,f).

We briefly note other factors relevant to the comparison of direct and virtual gates. *Multi-phonon encodings.* Direct gates require that qubits be encoded in the $|0,1\rangle$ phonon Fock states, while virtual operations are compatible with multi-phonon encodings, including some bosonic quantum error-correcting codes [58, 59]. *Parallelism.* Direct gates must be executed serially, while virtual gates can be executed in parallel by simultaneously applying the requisite drives (though care should be taken to ensure that the additional drives do not bring spurious couplings on resonance). *Speed.* Virtual gates are inherently slower than direct gates, with realistically attainable coupling rates $g_v/2\pi \sim 10-100\,\mathrm{kHz}$ [56].

qRAM Implementation.—To illustrate the advantages of cQAD systems, we propose an implementation of a qRAM [35, 36]. As defined by Eq.(1), a qRAM is a device which can query a database with an address in superposition. The ability to perform such queries efficiently is

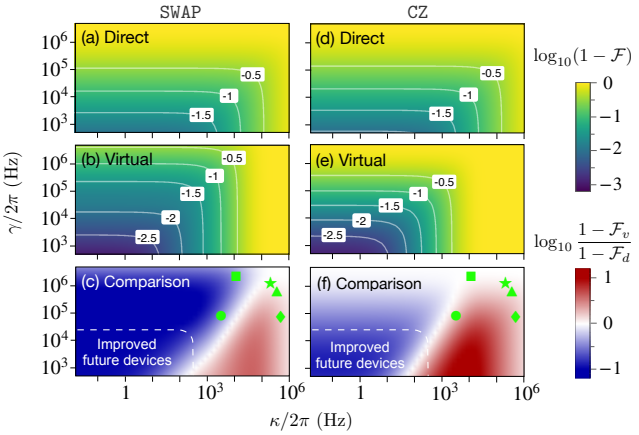

FIG. 3. Comparison of direct and virtual operations. (a,b) $\log_{10}(1-\mathcal{F})$ for the direct and virtual SWAP operations, respectively. The couplings are optimized subject to constraints ($g_d \in [0, g]$, constraints on g_v are discussed in [56]). (c) Comparison of direct and virtual SWAP operations. The log ratio of the infidelities is plotted, with the virtual operations attaining higher fidelities in the blue region. (d,e) Log_{10} infidelity for the direct and virtual CZ operations. (f) Comparison of CZ operations. For reference, the symbols {●,■,▲,♦,★} respectively denote the decoherence rates κ (phonon) and γ (transmon) measured in Refs. [17], [19], [25], [21], and [22]. Note, however, that the plots are generated using typical parameter values, not specific values from any one experiment. Parameters: $g/2\pi = 10$MHz, $\delta/2\pi = 100$MHz, $\nu/2\pi = 10$MHz, and $\Delta\nu/2\pi = 1$MHz.

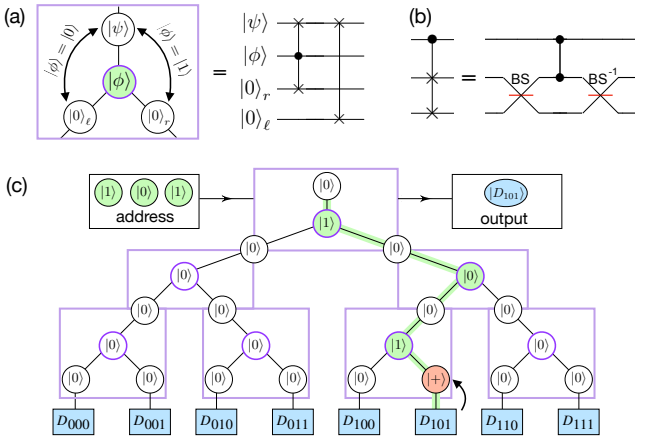

FIG. 4. cQAD implementation of qRAM. (a) Quantum router. Each circle represents a phonon mode. The router directs the qubit $|\psi\rangle$ in the incoming mode (top) to either the right or left mode conditioned on the state of the routing qubit $|\phi\rangle$. (b) Controlled SWAP. Note that this circuit implements the gate only within the relevant subspace of < 2 total phonons in the modes to be swapped. (c) qRAM implementation. Address qubits (green) are routed into position one-by-one, carving out a path to the database. The bus qubit (red) follows this path to retrieve the data D_j. The bus and address qubits are then routed back out of the tree to complete the query. The database (blue squares) can be either classical or quantum. In the former case, the bus is initially prepared in $|+\rangle$, and classical bits are copied to the bus by applying phase shifts to each mode at the bottom of the tree. In the latter case, the data qubit is extracted through a sequence of controlled SWAP operations. See [56] for details.

a prerequisite for a variety of quantum algorithms, including Grover's search [37], matrix inversion [38], and various proposals in the field of quantum machine learning [39]. While demanding hardware and connectivity requirements have thus far precluded an experimental demonstration of a qRAM, our proposed cQAD implementation is naturally hardware-efficient. Indeed, a small-scale cQAD qRAM can be implemented with a single multimode resonator.

The elementary building block of our qRAM implementation is a *quantum router*, shown in Fig. 4(a). The router directs an incoming qubit into different output modes conditioned on the state of a routing qubit. When the routing qubit is in state $|0\rangle$ ($|1\rangle$), an incoming qubit $|\psi\rangle$ in the top mode is swapped to the left(right) mode. The routers are implemented using the operations described above: the routing circuit contains a SWAP and a controlled-SWAP gate, the latter of which is implemented using CZ and beamsplitter operations (Fig. 4b).

To implement a qRAM, a collection of routers is arranged in a binary tree, with the outputs of routers at one level acting as inputs to routers at the next (Fig. 4c). To query the database at the bottom of the tree, qubits from the address register are routed sequentially into the tree, with earlier address qubits controlling the routing of later ones in a "bucket-brigade" scheme [35]. A "bus" qubit then follows the path paved by the address qubits and extracts the data, after which it is routed back out of the tree and into the output register. Finally, to disentangle the address and routers, the address qubits are routed back out of the tree. Since all routing operations are quantum-controlled, preparing the address register in superposition allows access to the data in superposition, thereby implementing operation (1). Further details are provided in [56].

We highlight three appealing properties of this cQAD-based qRAM.

1. *Hardware-efficiency.* Hundreds of phonon modes can simultaneously couple to a transmon on a single chip [16]. Thus, the hardware and fabrication cost of a cQAD-based qRAM can be drastically reduced in comparison to cavity- [36] or circuit-QED [60] implementations.

2. *Scalability.* It is not necessary to control all routing through a single transmon; since only adjacent routers are coupled, different regions of the tree can be controlled and implemented independently. For example, the qRAM can be built out of several modules, where each module comprises a group of routers controlled by one transmon. The phononic modes in each module could be supported in physically separate resonators, or mul-

tiple transmons could be simultaneously coupled to the same multimode resonator to give access to a large bandwidth of modes, potentially spanning several GHz [16].

3. *Error resilience.* Because our implementation follows the bucket-brigade model, it inherits a favorable $\log N$ error scaling [35, 36, 61]. In particular, the scaling argument of Ref. [35] directly applies to phonon-loss errors: the query infidelity scales as $1 - \mathcal{F} \sim \varepsilon \log N$, where ε is the phonon loss probability. Remarkably, one can show that the infidelity scales logarithmically for arbitrary independent, incoherent errors, such as phonon loss, dephasing, and heating [62].

Discussion.—We have proposed a quantum computing architecture for multimode cQAD and an implementation of a qRAM based on it. The implementation is hardware-efficient, owing to the compactness of multimode cQAD systems that is enabled by small acoustic wavelengths. We emphasize that hardware efficiency is not only crucial for scaling to large system sizes, but that it is also particularly advantageous for near-term experiments. Indeed, a small-scale qRAM can be implemented even with just a single multimode resonator. In the long term, the use of bosonic quantum error correcting codes [59, 63] and compatible logical gates [58, 64, 65] to implement a qRAM that is both fault-tolerant and hardware-efficient is an intriguing direction for future research. These ideas can also be directly applied to multimode cQED.

To be viable, our scheme requires long phonon coherence times ($1/\kappa \gg 1/g_v$). Though loss due to intrinsic material processes like phonon-phonon scattering or two level systems limit phonon coherence, such mechanisms should not prevent access to this regime. Indeed, both BAW and PC quality factors can approach 10^{10} before encountering such limits [27, 66, 67], corresponding to $\kappa/2\pi \sim 1$Hz at GHz frequencies. Additionally, intrinsic sources of phonon dephasing are not expected [68]. Phonon decoherence in current cQAD experiments is thus likely dominated by extrinsic mechanisms that can be mitigated with improved fabrication techniques, though the extent to which the coupling to superconducting circuits may limit phonon coherence in cQAD is an important open question.

Acknowledgements.—We thank Vijay Jain, Prashanta Kharel, Patricio Arrangoiz-Arriola, Alex Wollack, Hong Tang, Peter Rakich, and Oskar Painter for helpful discussions. C.T.H. acknowledges support from the NSF Graduate Research Fellowship Program (DGE1752134). We acknowledge support from the ARL-CDQI (W911NF-15-2-0067, W911NF-18-2-0237), ARO (W911NF-18-1-0020, W911NF-18-1-0212), ARO MURI (W911NF-16-1-0349), AFOSR MURI (FA9550-15-1-0015), DOE (DE-SC0019406), NSF (EFMA-1640959, DMR-1609326), and the Packard Foundation (2013-39273).

[1] A. Blais, J. Gambetta, A. Wallraff, D. I. Schuster, S. M. Girvin, M. H. Devoret, and R. J. Schoelkopf, Phys. Rev. A **75**, 032329 (2007).
[2] R. J. Schoelkopf and S. M. Girvin, Nature **451**, 664 (2008).
[3] M. Reagor, W. Pfaff, C. Axline, R. W. Heeres, N. Ofek, K. Sliwa, E. Holland, C. Wang, J. Blumoff, K. Chou, M. J. Hatridge, L. Frunzio, M. H. Devoret, L. Jiang, and R. J. Schoelkopf, Phys. Rev. B **94**, 014506 (2016).
[4] M. Hofheinz, E. M. Weig, M. Ansmann, R. C. Bialczak, E. Lucero, M. Neeley, A. D. O'Connell, H. Wang, J. M. Martinis, and A. N. Cleland, Nature **454**, 310 (2008).
[5] S. Krastanov, V. V. Albert, C. Shen, C.-L. Zou, R. W. Heeres, B. Vlastakis, R. J. Schoelkopf, and L. Jiang, Phys. Rev. A **92**, 040303(R) (2015).
[6] R. W. Heeres, P. Reinhold, N. Ofek, L. Frunzio, L. Jiang, M. H. Devoret, and R. J. Schoelkopf, Nat. Commun. **8**, 94 (2017).
[7] L. Sun, A. Petrenko, Z. Leghtas, B. Vlastakis, G. Kirchmair, K. M. Sliwa, A. Narla, M. Hatridge, S. Shankar, J. Blumoff, L. Frunzio, M. Mirrahimi, M. H. Devoret, and R. J. Schoelkopf, Nature **511**, 444 (2014).
[8] N. Ofek, A. Petrenko, R. Heeres, P. Reinhold, Z. Leghtas, B. Vlastakis, Y. Liu, L. Frunzio, S. M. Girvin, L. Jiang, M. Mirrahimi, M. H. Devoret, and R. J. Schoelkopf, Nature **536**, 441 (2016).
[9] L. Hu, Y. Ma, W. Cai, X. Mu, Y. Xu, W. Wang, Y. Wu, H. Wang, Y. P. Song, C.-L. Zou, S. M. Girvin, L.-M. Duan, and L. Sun, Nat. Phys. **15**, 503 (2019).
[10] K. Geerlings, S. Shankar, E. Edwards, L. Frunzio, R. J. Schoelkopf, and M. H. Devoret, Appl. Phys. Lett. **100**, 192601 (2012).
[11] J. Wenner, R. Barends, R. C. Bialczak, Y. Chen, J. Kelly, E. Lucero, M. Mariantoni, A. Megrant, P. J. J. O'Malley, D. Sank, A. Vainsencher, H. Wang, T. C. White, Y. Yin, J. Zhao, A. N. Cleland, and J. M. Martinis, Appl. Phys. Lett. **99**, 113513 (2011).
[12] A. Romanenko, R. Pilipenko, S. Zorzetti, D. Frolov, M. Awida, S. Posen, and A. Grassellino, ArXiv181003703 Cond-Mat Physicsphysics Physicsquant-Ph (2018), arXiv:1810.03703 [cond-mat, physics:physics, physics:quant-ph].
[13] A. D. O'Connell, M. Hofheinz, M. Ansmann, R. C. Bialczak, M. Lenander, E. Lucero, M. Neeley, D. Sank, H. Wang, M. Weides, J. Wenner, J. M. Martinis, and A. N. Cleland, Nature **464**, 697 (2010).
[14] J.-M. Pirkkalainen, S. U. Cho, J. Li, G. S. Paraoanu, P. J. Hakonen, and M. A. Sillanpää, Nature **494**, 211 (2013).
[15] M. V. Gustafsson, T. Aref, A. F. Kockum, M. K. Ekström, G. Johansson, and P. Delsing, Science **346**, 207 (2014).
[16] Y. Chu, P. Kharel, W. H. Renninger, L. D. Burkhart, L. Frunzio, P. T. Rakich, and R. J. Schoelkopf, Science **358**, 199 (2017).
[17] Y. Chu, P. Kharel, T. Yoon, L. Frunzio, P. T. Rakich, and R. J. Schoelkopf, Nature **563**, 666 (2018).
[18] M. Kervinen, I. Rissanen, and M. Sillanpää, Phys. Rev. B **97**, 205443 (2018).
[19] R. Manenti, A. F. Kockum, A. Patterson, T. Behrle, J. Rahamim, G. Tancredi, F. Nori, and P. J. Leek, Nat.

Commun. **8**, 975 (2017).
[20] A. Noguchi, R. Yamazaki, Y. Tabuchi, and Y. Nakamura, Phys. Rev. Lett. **119**, 180505 (2017).
[21] K. J. Satzinger, Y. P. Zhong, H.-S. Chang, G. A. Peairs, A. Bienfait, M.-H. Chou, A. Y. Cleland, C. R. Conner, É. Dumur, J. Grebel, I. Gutierrez, B. H. November, R. G. Povey, S. J. Whiteley, D. D. Awschalom, D. I. Schuster, and A. N. Cleland, Nature **563**, 661 (2018).
[22] B. A. Moores, L. R. Sletten, J. J. Viennot, and K. W. Lehnert, Phys. Rev. Lett. **120**, 227701 (2018).
[23] A. N. Bolgar, J. I. Zotova, D. D. Kirichenko, I. S. Besedin, A. V. Semenov, R. S. Shaikhaidarov, and O. V. Astafiev, Phys. Rev. Lett. **120**, 223603 (2018).
[24] L. R. Sletten, B. A. Moores, J. J. Viennot, and K. W. Lehnert, Phys. Rev. X **9**, 021056 (2019).
[25] P. Arrangoiz-Arriola, E. A. Wollack, Z. Wang, M. Pechal, W. Jiang, T. P. McKenna, J. D. Witmer, and A. H. Safavi-Naeini, Nature **571**, 537 (2019).
[26] A. H. Safavi-Naeini, D. V. Thourhout, R. Baets, and R. V. Laer, Optica **6**, 213 (2019).
[27] G. S. MacCabe, H. Ren, J. Luo, J. D. Cohen, H. Zhou, A. Sipahigil, M. Mirhosseini, and O. Painter, arXiv:1901.04129.
[28] M. J. A. Schuetz, E. M. Kessler, G. Giedke, L. M. K. Vandersypen, M. D. Lukin, and J. I. Cirac, Phys. Rev. X **5**, 031031 (2015).
[29] A. N. Cleland and M. R. Geller, Phys. Rev. Lett. **93**, 070501 (2004).
[30] A. Bienfait, K. J. Satzinger, Y. P. Zhong, H.-S. Chang, M.-H. Chou, C. R. Conner, É. Dumur, J. Grebel, G. A. Peairs, R. G. Povey, and A. N. Cleland, Science **364**, 368 (2019).
[31] L. Guo, A. Grimsmo, A. F. Kockum, M. Pletyukhov, and G. Johansson, Phys. Rev. A **95**, 053821 (2017).
[32] G. Andersson, B. Suri, L. Guo, T. Aref, and P. Delsing, arXiv:1812.01302.
[33] M. Pechal, P. Arrangoiz-Arriola, and A. H. Safavi-Naeini, Quantum Sci. Technol. **4**, 015006 (2018).
[34] R. K. Naik, N. Leung, S. Chakram, P. Groszkowski, Y. Lu, N. Earnest, D. C. McKay, J. Koch, and D. I. Schuster, Nat. Commun. **8**, 1904 (2017).
[35] V. Giovannetti, S. Lloyd, and L. Maccone, Phys. Rev. Lett. **100**, 160501 (2008).
[36] V. Giovannetti, S. Lloyd, and L. Maccone, Phys. Rev. A **78**, 052310 (2008).
[37] L. K. Grover, Phys. Rev. Lett. **79**, 325 (1997).
[38] A. W. Harrow, A. Hassidim, and S. Lloyd, Phys. Rev. Lett. **103**, 150502 (2009).
[39] J. Biamonte, P. Wittek, N. Pancotti, P. Rebentrost, N. Wiebe, and S. Lloyd, Nature **549**, 195 (2017).
[40] M. Mariantoni, H. Wang, T. Yamamoto, M. Neeley, R. C. Bialczak, Y. Chen, M. Lenander, E. Lucero, A. D. O'Connell, D. Sank, M. Weides, J. Wenner, Y. Yin, J. Zhao, A. N. Korotkov, A. N. Cleland, and J. M. Martinis, Science **334**, 61 (2011).
[41] N. Jiang, Y.-F. Pu, W. Chang, C. Li, S. Zhang, and L.-M. Duan, Npj Quantum Inf. **5**, 28 (2019).
[42] R. Manenti, M. J. Peterer, A. Nersisyan, E. B. Magnusson, A. Patterson, and P. J. Leek, Phys. Rev. B **93**, 041411(R) (2016).
[43] T. Aref, P. Delsing, M. K. Ekström, A. F. Kockum, M. V. Gustafsson, G. Johansson, P. J. Leek, E. Magnusson, and R. Manenti, in *Superconducting Devices in Quantum Optics*, edited by R. H. Hadfield and G. Johansson (Springer International Publishing, Cham, 2016) pp. 217–244.
[44] W. H. Renninger, P. Kharel, R. O. Behunin, and P. T. Rakich, Nat. Phys. **14**, 601 (2018).
[45] P. Kharel, Y. Chu, M. Power, W. H. Renninger, R. J. Schoelkopf, and P. T. Rakich, APL Photonics **3**, 066101 (2018).
[46] X. Han, C.-L. Zou, and H. X. Tang, Phys. Rev. Lett. **117**, 123603 (2016).
[47] T. A. Palomaki, J. W. Harlow, J. D. Teufel, R. W. Simmonds, and K. W. Lehnert, Nature **495**, 210 (2013).
[48] M. Pechal, L. Huthmacher, C. Eichler, S. Zeytinoğlu, A. A. Abdumalikov, S. Berger, A. Wallraff, and S. Filipp, Phys. Rev. X **4**, 041010 (2014).
[49] S. J. Srinivasan, N. M. Sundaresan, D. Sadri, Y. Liu, J. M. Gambetta, T. Yu, S. M. Girvin, and A. A. Houck, Phys. Rev. A **89**, 033857 (2014).
[50] C. J. Axline, L. D. Burkhart, W. Pfaff, M. Zhang, K. Chou, P. Campagne-Ibarcq, P. Reinhold, L. Frunzio, S. M. Girvin, L. Jiang, M. H. Devoret, and R. J. Schoelkopf, Nat. Phys. **14**, 705 (2018).
[51] P. Kurpiers, P. Magnard, T. Walter, B. Royer, M. Pechal, J. Heinsoo, Y. Salathé, A. Akin, S. Storz, J.-C. Besse, S. Gasparinetti, A. Blais, and A. Wallraff, Nature **558**, 264 (2018).
[52] J. Y. Mutus, T. C. White, E. Jeffrey, D. Sank, R. Barends, J. Bochmann, Y. Chen, Z. Chen, B. Chiaro, A. Dunsworth, J. Kelly, A. Megrant, C. Neill, P. J. J. O'Malley, P. Roushan, A. Vainsencher, J. Wenner, I. Siddiqi, R. Vijay, A. N. Cleland, and J. M. Martinis, Appl Phys Lett **103**, 122602 (2013).
[53] Z. Leghtas, S. Touzard, I. M. Pop, A. Kou, B. Vlastakis, A. Petrenko, K. M. Sliwa, A. Narla, S. Shankar, M. J. Hatridge, M. Reagor, L. Frunzio, R. J. Schoelkopf, M. Mirrahimi, and M. H. Devoret, Science **347**, 853 (2015).
[54] Y. Y. Gao, B. J. Lester, Y. Zhang, C. Wang, S. Rosenblum, L. Frunzio, L. Jiang, S. M. Girvin, and R. J. Schoelkopf, Phys. Rev. X **8**, 021073 (2018).
[55] Y. Zhang, B. J. Lester, Y. Y. Gao, L. Jiang, R. J. Schoelkopf, and S. M. Girvin, Phys. Rev. A **99**, 012314 (2019).
[56] See Supplementary Material at [URL], which includes Refs. [69–78].
[78] N. K. Langford, S. Ramelow, R. Prevedel, W. J. Munro, G. J. Milburn, and A. Zeilinger, Nature **478**, 360 (2011).
[58] M. Y. Niu, I. L. Chuang, and J. H. Shapiro, Phys. Rev. Lett. **120**, 160502 (2018).
[59] M. Y. Niu, I. L. Chuang, and J. H. Shapiro, Phys. Rev. A **97**, 032323 (2018).
[60] T. H. Kyaw, S. Felicetti, G. Romero, E. Solano, and L.-C. Kwek, Sci. Rep. **5**, 8621 (2015).
[61] S. Arunachalam, V. Gheorghiu, T. Jochym-O'Connor, M. Mosca, and P. V. Srinivasan, New J. Phys. **17**, 123010 (2015).
[62] C. T. Hann and L. Jiang, (in preparation).
[63] V. V. Albert, K. Noh, K. Duivenvoorden, D. J. Young, R. T. Brierley, P. Reinhold, C. Vuillot, L. Li, C. Shen, S. M. Girvin, B. M. Terhal, and L. Jiang, Phys. Rev. A **97**, 032346 (2018).
[64] H. K. Lau and M. B. Plenio, Phys Rev Lett **117**, 100501 (2016).
[65] Y. Y. Gao, B. J. Lester, K. S. Chou, L. Frunzio, M. H.

Devoret, L. Jiang, S. M. Girvin, and R. J. Schoelkopf, Nature **566**, 509 (2019).
[66] M. Goryachev, D. L. Creedon, E. N. Ivanov, S. Galliou, R. Bourquin, and M. E. Tobar, Appl. Phys. Lett. **100**, 243504 (2012).
[67] S. Galliou, M. Goryachev, R. Bourquin, P. Abbé, J. P. Aubry, and M. E. Tobar, Sci. Rep. **3**, 2132 (2013).
[68] T. Faust, J. Rieger, M. J. Seitner, J. P. Kotthaus, and E. M. Weig, Nat. Phys. **9**, 485 (2013).
[69] S. E. Nigg, H. Paik, B. Vlastakis, G. Kirchmair, S. Shankar, L. Frunzio, M. H. Devoret, R. J. Schoelkopf, and S. M. Girvin, Phys. Rev. Lett. **108**, 240502 (2012).
[70] P. Kharel, G. I. Harris, E. A. Kittlaus, W. H. Renninger, N. T. Otterstrom, J. G. E. Harris, and P. T. Rakich, arXiv:1809.04020.
[71] C. Axline, M. Reagor, R. Heeres, P. Reinhold, C. Wang, K. Shain, W. Pfaff, Y. Chu, L. Frunzio, and R. J. Schoelkopf, Appl. Phys. Lett. **109**, 042601 (2016).
[72] R. Babbush, C. Gidney, D. W. Berry, N. Wiebe, J. McClean, A. Paler, A. Fowler, and H. Neven, Phys. Rev. X **8**, 041015 (2018), arXiv:1805.03662.
[73] S. Chakraborty, A. Gilyén, and S. Jeffery, arXiv:1804.01973.
[74] A. Gilyén, Y. Su, G. H. Low, and N. Wiebe, arXiv:1806.01838.
[75] R. Barends, J. Kelly, A. Megrant, A. Veitia, D. Sank, E. Jeffrey, T. C. White, J. Mutus, A. G. Fowler, B. Campbell, Y. Chen, Z. Chen, B. Chiaro, A. Dunsworth, C. Neill, P. O'Malley, P. Roushan, A. Vainsencher, J. Wenner, A. N. Korotkov, A. N. Cleland, and J. M. Martinis, Nature **508**, 500 (2014).
[76] K. Wright, K. M. Beck, S. Debnath, J. M. Amini, Y. Nam, N. Grzesiak, J.-S. Chen, N. C. Pisenti, M. Chmielewski, C. Collins, K. M. Hudek, J. Mizrahi, J. D. Wong-Campos, S. Allen, J. Apisdorf, P. Solomon, M. Williams, A. M. Ducore, A. Blinov, S. M. Kreikemeier, V. Chaplin, M. Keesan, C. Monroe, and J. Kim, arXiv:1903.08181.
[77] L. Bishop, S. Bravyi, A. W. Cross, J. M. Gambetta, and J. A. Smolin, IBM (2017).
[78] E. Knill, R. Laflamme, and G. J. Milburn, Nature **409**, 46 (2001).